Report

Current Biology

# Hexadirectional Modulation of High-Frequency Electrophysiological Activity in the Human Anterior Medial Temporal Lobe Maps Visual Space

## Highlights

- Hexadirectional modulation of human high-frequency electrophysiological activity
- Grid-like mapping of visual space in the human entorhinal cortex
- Grid-coding beyond environmental mapping during locomotion

## Authors

Tobias Staudigl, Marcin Leszczynski, Joshua Jacobs, Sameer A. Sheth, Charles E. Schroeder, Ole Jensen, Christian F. Doeller

## Correspondence

tobias.staudigl@cshs.org (T.S.), doeller@cbs.mpg.de (C.F.D.)

## In Brief

Staudigl et al. show grid-like modulation of human high-frequency activity in non-invasive magnetoencephalographic and intracranial EEG recordings. The results indicate that the human entorhinal cortex codes visual space in a grid-like manner, supporting the view that grid coding generalizes beyond environmental mapping during locomotion.

Staudigl et al., 2018, Current Biology *28*, 1–5
October 22, 2018 
https://doi.org/10.1016/j.cub.2018.09.035

CellPress

Please cite this article in press as: Staudigl et al., Hexadirectional Modulation of High-Frequency Electrophysiological Activity in the Human Anterior Medial Temporal Lobe Maps Visual Space, Current Biology (2018), https://doi.org/10.1016/j.cub.2018.09.035

Current Biology
Report



# Hexadirectional Modulation of High-Frequency Electrophysiological Activity in the Human Anterior Medial Temporal Lobe Maps Visual Space

Tobias Staudigl,[1,2,9,*] Marcin Leszczynski,[3,4] Joshua Jacobs,[5] Sameer A. Sheth,[3] Charles E. Schroeder,[3,4] Ole Jensen,[6] and Christian F. Doeller[7,8,*]
[1]Donders Institute for Brain, Cognition, and Behaviour, Radboud University, Nijmegen, the Netherlands
[2]Department of Neurosurgery, Cedars-Sinai Medical Center, Los Angeles, CA, USA
[3]Cognitive Science and Neuromodulation Program, Department of Neurological Surgery, Columbia University College of Physicians and Surgeons, New York, NY, USA
[4]Translational Neuroscience Division, Nathan Kline Institute, Orangeburg, NY, USA
[5]Department of Biomedical Engineering, Columbia University, New York, NY, USA
[6]Centre for Human Brain Health, School of Psychology, University of Birmingham, Birmingham, UK
[7]Kavli Institute for Systems Neuroscience, Centre for Neural Computation, The Egil and Pauline Braathen and Fred Kavli Centre for Cortical Microcircuits, Norwegian University of Science and Technology (NTNU), Trondheim, Norway
[8]Max Planck Institute for Human Cognitive and Brain Sciences, Leipzig, Germany
[9]Lead Contact
*Correspondence: tobias.staudigl@cshs.org (T.S.), doeller@cbs.mpg.de (C.F.D.)
https://doi.org/10.1016/j.cub.2018.09.035

## SUMMARY

Grid cells are one of the core building blocks of spatial navigation [1]. Single-cell recordings of grid cells in the rodent entorhinal cortex revealed hexagonal coding of the local environment during spatial navigation [1]. Grid-like activity has also been identified in human single-cell recordings during virtual navigation [2]. Human fMRI studies further provide evidence that grid-like signals are also accessible on a macroscopic level [3–7]. Studies in both non-human primates [8] and humans [9, 10] suggest that grid-like coding in the entorhinal cortex generalizes beyond spatial navigation during locomotion, providing evidence for grid-like mapping of visual space during visual exploration—akin to the grid cell positional code in rodents during spatial navigation. However, electrophysiological correlates of the grid code in humans remain unknown. Here, we provide evidence for grid-like, hexadirectional coding of visual space by human high-frequency activity, based on two independent datasets: non-invasive magnetoencephalography (MEG) in healthy subjects and entorhinal intracranial electroencephalography (EEG) recordings in an epileptic patient. Both datasets consistently show a hexadirectional modulation of broadband high-frequency activity (60–120 Hz). Our findings provide first evidence for a grid-like MEG signal, indicating that the human entorhinal cortex codes visual space in a grid-like manner [8–10], and support the view that grid coding generalizes beyond environmental mapping during locomotion [4–6, 11]. Due to their millisecond accuracy, MEG recordings allow linking of grid-like activity to epochs during relevant behavior, thereby opening up the possibility for new MEG-based investigations of grid coding at high temporal resolution.

## RESULTS

The present study set out to investigate the electrophysiological basis of grid-like, hexadirectional coding during visual exploration in humans by simultaneously recording magnetoencephalography (MEG) and eye-tracking data from 35 healthy participants during free viewing of natural scenes (Figure 1A) and by simultaneously recording intracranial electroencephalography (EEG) and eye-tracking data with depth electrodes in the entorhinal cortex of one epilepsy patient (Figure S1). Although the exact physiology of the broadband high-frequency activity (BHA) remains to be discovered, it has been shown to correlate with local neural activity [12–15]. Building on this and other work demonstrating high-frequency activity in the entorhinal cortex of behaving rodents [16], we hypothesized to find a grid-like modulation of neuromagnetic BHA in the anterior medial temporal lobe (MTL; Figure 1B) and sought to verify the MEG findings in the intracranial recordings.

### Grid-like Modulation of Source-Localized Broadband High-Frequency MEG Data Maps Visual Space

MEG data were aligned to saccade onsets (Figure 1A), and BHA power (60–120 Hz) source localized to the anterior MTL (Figure 1B) was extracted during saccadic eye movements. We used a recently optimized MTL source-reconstruction method [17], extending prior MEG work localizing MTL activity [18–22]. Applying a quadrature filter approach [3], we estimated the phase of hexadirectional activity as a function of saccade direction (putative "grid orientation") and subsequently quantified BHA power aligned and misaligned to the main grid axis, in a

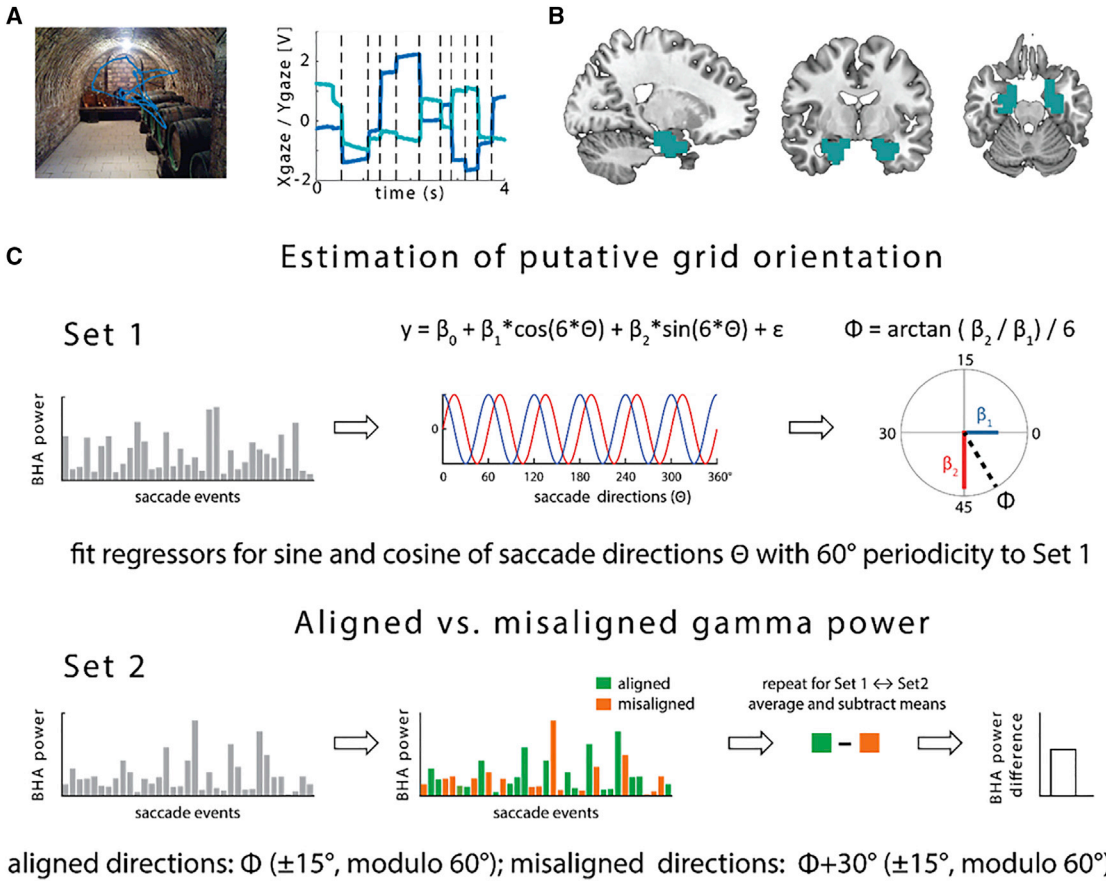


**Figure 1. Hexadirectional Mapping of Visual Space: Procedure and Analysis**

(A) Paradigm: free viewing of 100 indoor and 100 outdoor scenes with simultaneous eye tracking (left). MEG data are aligned to saccade onsets, defining events of interest (right).

(B) Region of interest (highlighted), comprising bilateral anterior portions of the hippocampus and parahippocampal gyrus.

(C) Analysis rationale. Data were split into halves (set 1 and set 2) to estimate the putative grid orientation (angle of hexadirectional activity) separately from computing aligned and misaligned BHA power, in a two-fold cross-validation design. Estimation of putative grid orientation was done by fitting regressors for sine and cosine of saccade directions (Θ) in the respective rotational symmetric space (here: 60° periodicity) to set 1 BHA power (the general linear model included a constant and saccade duration as nuisance regressors). Resulting beta estimates were used to derive the putative grid orientation angle (Φ). Trials in set 2 were split according saccade directions aligned versus misaligned to Φ. The difference in BHA power (aligned − misaligned) reflects the grid-like modulation of BHA power.

two-fold cross-validation design (Figure 1C). Estimation of the putative grid orientation was achieved by fitting regressors for the sine and cosine of each saccade direction Φ in the respective rotational symmetric space (e.g., 60°, 6-fold periodicity, along with biologically implausible 4-, 5-, 7-, and 8-fold control periodicities) to one half of the data (set 1) in a general linear model. Saccade length was included as a nuisance regressor in the analysis. The resulting phase angle was extracted from the obtained beta coefficients (Φ = arctan(β2/β1) / symmetry), in the respective rotational symmetric space. The other half of the data (set 2) was binned according to Θ, into aligned bins (Φ ± 15°, modulo 60°) and misaligned bins (Φ +30° ± 15°, modulo 60°). This procedure was repeated after swapping set 1 and set 2, and power was averaged across the repetitions for aligned and misaligned bins, respectively.

We found significantly higher 60° periodic BHA (60–120 Hz) for aligned versus misaligned directional sampling in the left anterior MTL, including entorhinal cortex ($t_{34}$ = 4.53, p < 0.00007; Figure 2A; Cohen's d = 0.1988, reflecting a small effect size). When the six aligned and six misaligned 30° bins were inspected, aligned directions generally elicited higher BHA power than misaligned directions (Figure 2B), indicating that the effect is not driven by a single direction. The putative grid orientations (i.e., the angle of the hexadirectional modulation) did not cluster across participants (Figure 2D). A 2 × 5 repeated-measures ANOVA with factors alignment (aligned versus misaligned) and rotational symmetry (4-, 5-, 6-, 7-, and 8-fold) revealed a significant interaction ($F_{3.305,\ 112.3,\ \text{Greenhouse-Geisser}}$ = 3.49, p < 0.015). Importantly, the significant quadratic contrast (quadratic F = 10.8, p < 0.0025; linear and cubic contrasts not significant) indicated a u-inverted shape of the differences across the rotational symmetries, being optimal for the 6-fold symmetry. Planned post hoc comparisons revealed that the difference for the 6-fold symmetry was bigger than for any of the other symmetries (all $t_{34}$ values > 2.26, all p values < 0.03, two sided, uncorrected). Moreover, the differences for 4-, 5-, 7-,

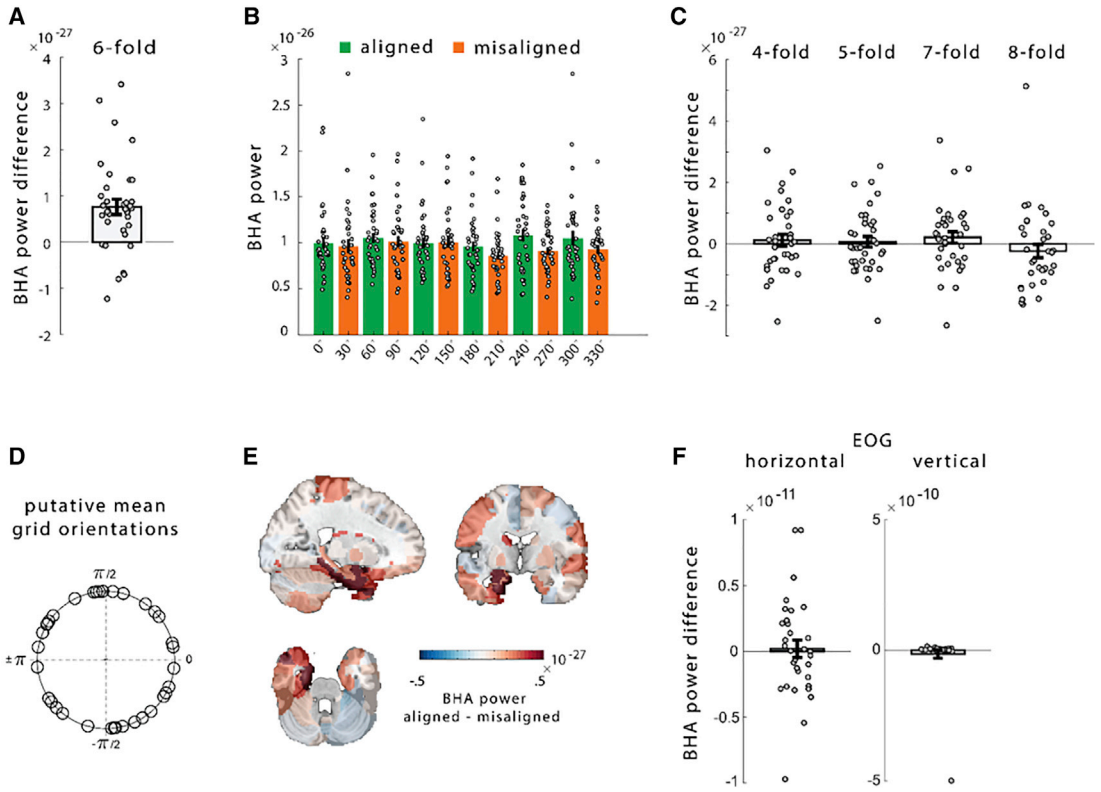


**Figure 2. Grid-like Modulation of BHA MEG Activity during Visual Exploration**

(A) BHA power (60–120 Hz) aligned to the putative grid orientation is significantly higher than misaligned BHA power in the left anterior MTL.

(B) 6-fold symmetric modulation of the BHA power, visualizing the effect in (A). The x axis depicts the difference between saccade directions and the estimated putative grid orientations.

(C) Other rotational symmetries (4-, 5-, 7-, and 8-fold) do not show significant differences between aligned and misaligned BHA power

(D) Putative grid orientations across participants did not show clustering.

(E) Whole-brain analysis shows clustering of highest differences (aligned versus misaligned, 60–120 Hz, 6-fold symmetry) in the left temporal lobe.

(F) No significant difference between aligned versus misaligned BHA power, in horizontal or vertical electrooculogram (EOG) data (available in 32 participants).

Dots show data from all participants; error bars show SEM. See also Figures S1 and S2.

and 8-fold symmetry were not significantly different from zero (all $t_{34}$ values < 1.2 and > −1.1, all p values > 0.27, two sided, uncorrected; Figure 2E). A repeated-measures ANOVA for the aligned bins in the MEG data showed no significant difference ($F_{34,5}$ = 2.05, p = 0.075). A repeated-measures ANOVA comparing the difference (aligned − misaligned) across bins indicated that the effect was more pronounced for some directions ($F_{34,5}$ = 2.28, p = 0.049). No 6-fold modulation of BHA power was observed in right anterior MTL ($t_{34}$ = −0.4, p > 0.68).

In addition, a whole-brain analysis of the 60° periodic modulation confirms the findings from the region of interest (ROI)-based analysis and shows clustering of the highest differences between aligned and misaligned BHA power in the left MTL (Figure 2E), supporting the spatial specificity of the effect. To investigate whether the hexadirectional modulation was limited to BHA, we computed the 60° periodic modulation of power in a lower-frequency band (20–50 Hz). There was no significant difference between aligned versus misaligned directional sampling in the left anterior MTL ($t_{34}$ = 1.179, p = 0.247). Furthermore, in the present analyses, we investigated MEG activity during eye movements, which may be affected by oculomotor-related artifacts. However, a 60° periodic BHA power modulation could not be found when oculomotor activity recorded via electrooculogram (EOG) electrodes was analyzed ($t_{34}$ = 0.296, p > 0.769; $t_{34}$ = −0.9347, p > 0.357; for horizontal and vertical EOG signals, respectively; Figure 2F). Moreover, there was no significant difference in number of saccades aligned to the putative grid orientation versus number of saccades misaligned for 4-, 5-, 6-, 7-, and 8-fold rotational symmetries (see Figure S2).

In order to investigate the possible electrophysiological origin and spatial specificity of the MEG results, we analyzed intracranial data recorded from the entorhinal cortex of an epilepsy patient (Figure S1A) while the patient was performing a free-viewing task. The BHA power difference (aligned − misaligned) was significantly higher compared to a surrogate distribution in the 6-fold rotational symmetry (p < 0.011, one sided; Figures S1B and S1C). Biologically implausible 4-, 5-, 7-, and 8-fold symmetries did not show a significant modulation of BHA power (all p values > 0.36, one sided; Figure S1D), nor did a spatially adjacent amygdala electrode (Figure S1E) show a 6-fold rotational symmetry of BHA (p > 0.36; Figures S1E and S1G). The difference between the hexadirectional modulation of BHA in entorhinal cortex and amygdala was significantly higher than expected by chance (p < 0.013).

## DISCUSSION

The present results provide the first evidence for a grid-like signal in non-invasive electrophysiological recordings in humans: electromagnetic activity, source localized to the anterior MTL, revealed a hexadirectional modulation of BHA power (60–120 Hz). Confirming these findings, intracranial field potentials recorded in the entorhinal cortex of a patient also showed a hexadirectional modulation of BHA power in the same frequency band. The whole-brain MEG and control analyses in the intracranial data point toward the spatial specificity of the effect within the anterior MTL (including the entorhinal cortex). The millisecond accuracy of these recordings allows us to link activity to epochs during the relevant behavior, thereby overcoming limitations of other non-invasive techniques, such as fMRI. We found a grid-like pattern in BHA power, which has been suggested to correlate with local neural activity [12–15], indicating that grid coding is detectable with mass-electrophysiological recordings, opening up the possibility for new non-invasive investigations of grid coding in cognitive neuroscience at high temporal resolution. We show that the grid-like modulation of electromagnetic and intracranial electrophysiological activity is related to the exploration of visual space. This is in line with work in non-human primates identifying cells in the MTL that fire in relation to the animal's gaze position [8, 23–25], rather than coding location during locomotion, as well as very recent fMRI work in humans showing hexadirectional modulations of entorhinal BOLD activity related to the exploration of visual space [9, 10]. Given the fundamental differences in sensory dominance between rodents and primates, it seems plausible that primates code location during exploration by locomotion and eye movements.

In sum, our results support the view that grid-like coding in the anterior MTL goes beyond mapping the environment during locomotion [8–10] and that the grid cell system could provide a general neural code underlying core cognitive functions in humans [4–6, 11].

## STAR★METHODS

Detailed methods are provided in the online version of this paper and include the following:

- KEY RESOURCES TABLE
- CONTACT FOR REAGENT AND RESOURCE SHARING
- EXPERIMENTAL MODEL AND SUBJECT DETAILS
- METHOD DETAILS
  - Design, Procedure and Materials
  - MEG Acquisition and Preprocessing
  - Eye Tracking Acquisition, Analyses and Trial Definition
  - Source Reconstruction
  - Hexadirectional analysis
  - Intracranial data
- QUANTIFICATION AND STATISTICAL ANALYSIS
- DATA AND SOFTWARE AVAILABILITY

### SUPPLEMENTAL INFORMATION

Supplemental Information includes two figures and can be found with this article online at https://doi.org/10.1016/j.cub.2018.09.035.

### ACKNOWLEDGMENTS

We thank all of the participants, in particular the patient, for taking part in the study; Elliot Smith for his help with intracranial data collection; and the medical staff at the Department of Neurological Surgery, Columbia University, for their support. This project has received funding from the European Union's Horizon 2020 research and innovation program under grant agreement no. 661373 (Marie Curie grant awarded to T.S.). C.F.D.'s research is supported by the Max Planck Society, the Kavli Foundation, the European Research Council (ERC-CoG GEOCOG 724836), the Centre of Excellence scheme of the Research Council of Norway—Centre for Neural Computation (223262/F50), the Egil and Pauline Braathen and Fred Kavli Centre for Cortical Microcircuits, the National Infrastructure scheme of the Research Council of Norway—NORBRAIN (197467/F50), and the Netherlands Organisation for Scientific Research (NWO-Vidi 452-12-009, NWO-Gravitation 024-001-006, NWO-MaGW 406-14-114, and NWO-MaGW 406-15-291). J.J. received funding from the US NIH (R01-MH104606 and S10 OD018211) and the National Science Foundation (BCS-1724243). C.E.S. received funding from the J.S. McDonnell Foundation and the US NIH (P50-MH109429, EY024776, and U01-NS098976). S.A.S. received funding from the Dana Foundation and the US NIH (MH 106700). O.J. received funding from the James S. McDonnell Foundation (220020448), the Wellcome Trust (207550), and the Royal Society Wolfson Research Merit Award.

### AUTHOR CONTRIBUTIONS

T.S., O.J., and C.F.D. designed the experiment. T.S., O.J., and C.F.D. wrote the paper. T.S. collected the data. T.S. performed the analyses. M.L. and C.E.S. designed, conducted the intracranial EEG part of the study and assisted in writing of the manuscript. S.A.S. implanted electrodes. J.J. provided electrode imaging information.

### DECLARATION OF INTERESTS

The authors declare no competing interests.

Received: April 19, 2018
Revised: July 2, 2018
Accepted: September 15, 2018
Published: October 11, 2018

### REFERENCES

1. Hafting, T., Fyhn, M., Molden, S., Moser, M.-B., and Moser, E.I. (2005). Microstructure of a spatial map in the entorhinal cortex. Nature *436*, 801–806.
2. Jacobs, J., Weidemann, C.T., Miller, J.F., Solway, A., Burke, J.F., Wei, X.X., Suthana, N., Sperling, M.R., Sharan, A.D., Fried, I., and Kahana, M.J. (2013). Direct recordings of grid-like neuronal activity in human spatial navigation. Nat. Neurosci. *16*, 1188–1190.
3. Doeller, C.F., Barry, C., and Burgess, N. (2010). Evidence for grid cells in a human memory network. Nature *463*, 657–661.
4. Bellmund, J.L., Deuker, L., Navarro Schröder, T., and Doeller, C.F. (2016). Grid-cell representations in mental simulation. eLife *5*, e17089.
5. Horner, A.J., Bisby, J.A., Zotow, E., Bush, D., and Burgess, N. (2016). Grid-like processing of imagined navigation. Curr. Biol. *26*, 842–847.
6. Constantinescu, A.O., O'Reilly, J.X., and Behrens, T.E.J. (2016). Organizing conceptual knowledge in humans with a gridlike code. Science *352*, 1464–1468.
7. Kunz, L., Schröder, T.N., Lee, H., Montag, C., Lachmann, B., Sariyska, R., Reuter, M., Stirnberg, R., Stöcker, T., Messing-Floeter, P.C., et al. (2015). Reduced grid-cell-like representations in adults at genetic risk for Alzheimer's disease. Science *350*, 430–433.
8. Killian, N.J., Jutras, M.J., and Buffalo, E.A. (2012). A map of visual space in the primate entorhinal cortex. Nature *491*, 761–764.

9. Nau, M., Navarro Schröder, T., Bellmund, J.L.S., and Doeller, C.F. (2018). Hexadirectional coding of visual space in human entorhinal cortex. Nat. Neurosci. *21*, 188–190.
10. Julian, J.B., Keinath, A.T., Frazzetta, G., and Epstein, R.A. (2018). Human entorhinal cortex represents visual space using a boundary-anchored grid. Nat. Neurosci. *21*, 191–194.
11. Wilming, N., König, P., König, S., and Buffalo, E.A. (2018). Entorhinal cortex receptive fields are modulated by spatial attention, even without movement. eLife *7*, e31745.
12. Ray, S., Crone, N.E., Niebur, E., Franaszczuk, P.J., and Hsiao, S.S. (2008). Neural correlates of high-gamma oscillations (60-200 Hz) in macaque local field potentials and their potential implications in electrocorticography. J. Neurosci. *28*, 11526–11536.
13. Mukamel, R., Gelbard, H., Arieli, A., Hasson, U., Fried, I., and Malach, R. (2005). Coupling between neuronal firing, field potentials, and FMRI in human auditory cortex. Science *309*, 951–954.
14. Manning, J.R., Jacobs, J., Fried, I., and Kahana, M.J. (2009). Broadband shifts in local field potential power spectra are correlated with single-neuron spiking in humans. J. Neurosci. *29*, 13613–13620.
15. Lachaux, J.-P., Axmacher, N., Mormann, F., Halgren, E., and Crone, N.E. (2012). High-frequency neural activity and human cognition: past, present and possible future of intracranial EEG research. Prog. Neurobiol. *98*, 279–301.
16. Chrobak, J.J., and Buzsáki, G. (1998). Gamma oscillations in the entorhinal cortex of the freely behaving rat. J. Neurosci. *18*, 388–398.
17. Backus, A.R., Schoffelen, J.M., Szebényi, S., Hanslmayr, S., and Doeller, C.F. (2016). Hippocampal-prefrontal theta oscillations support memory integration. Curr. Biol. *26*, 450–457.
18. Kaplan, R., Doeller, C.F., Barnes, G.R., Litvak, V., Düzel, E., Bandettini, P.A., and Burgess, N. (2012). Movement-related theta rhythm in humans: coordinating self-directed hippocampal learning. PLoS Biol. *10*, e1001267.
19. Fuentemilla, L., Barnes, G.R., Düzel, E., and Levine, B. (2014). Theta oscillations orchestrate medial temporal lobe and neocortex in remembering autobiographical memories. Neuroimage *85*, 730–737.
20. Staudigl, T., and Hanslmayr, S. (2013). Theta oscillations at encoding mediate the context-dependent nature of human episodic memory. Curr. Biol. *23*, 1101–1106.
21. Heusser, A.C., Poeppel, D., Ezzyat, Y., and Davachi, L. (2016). Episodic sequence memory is supported by a theta-gamma phase code. Nat. Neurosci. *19*, 1374–1380.
22. Guitart-Masip, M., Barnes, G.R., Horner, A., Bauer, M., Dolan, R.J., and Duzel, E. (2013). Synchronization of medial temporal lobe and prefrontal rhythms in human decision making. J. Neurosci. *33*, 442–451.
23. Rolls, E.T., Robertson, R.G., and Georges-François, P. (1997). Spatial view cells in the primate hippocampus. Eur. J. Neurosci. *9*, 1789–1794.
24. Wirth, S., Baraduc, P., Planté, A., Pinède, S., and Duhamel, J.-R. (2017). Gaze-informed, task-situated representation of space in primate hippocampus during virtual navigation. PLoS Biol. *15*, e2001045.
25. Meister, M.L.R., and Buffalo, E.A. (2018). Neurons in primate entorhinal cortex represent gaze position in multiple spatial reference frames. J. Neurosci. *38*, 2430–2441.
26. Berens, P. (2009). CircStat: a MATLAB toolbox for circular statistics. J. Stat. Softw. *31*, 1–21.
27. Oostenveld, R., Fries, P., Maris, E., and Schoffelen, J.M. (2011). FieldTrip: open source software for advanced analysis of MEG, EEG, and invasive electrophysiological data. Comput. Intell. Neurosci. *2011*, 156869.
28. Penny, W.D., Friston, K.J., Ashburner, J.T., Kiebel, S.J., and Nichols, T.E. (2011). Statistical Parametric Mapping: The Analysis of Functional Brain Images (Elsevier).
29. Avants, B.B., Tustison, N., and Song, G. (2009). Advanced normalization tools (ANTS). Insight J. *2*, 1–35.
30. Staudigl, T., Hartl, E., Noachtar, S., Doeller, C.F., and Jensen, O. (2017). Saccades are phase-locked to alpha oscillations in the occipital and medial temporal lobe during successful memory encoding. PLoS Biol. *15*, e2003404.
31. Stolk, A., Todorovic, A., Schoffelen, J.M., and Oostenveld, R. (2013). Online and offline tools for head movement compensation in MEG. Neuroimage *68*, 39–48.
32. Engbert, R., and Kliegl, R. (2003). Microsaccades uncover the orientation of covert attention. Vision Res. *43*, 1035–1045.
33. Tzourio-Mazoyer, N., Landeau, B., Papathanassiou, D., Crivello, F., Etard, O., Delcroix, N., Mazoyer, B., and Joliot, M. (2002). Automated anatomical labeling of activations in SPM using a macroscopic anatomical parcellation of the MNI MRI single-subject brain. Neuroimage *15*, 273–289.
34. Nolte, G. (2003). The magnetic lead field theorem in the quasi-static approximation and its use for magnetoencephalography forward calculation in realistic volume conductors. Phys. Med. Biol. *48*, 3637–3652.
35. Gross, J., Kujala, J., Hamalainen, M., Timmermann, L., Schnitzler, A., and Salmelin, R. (2001). Dynamic imaging of coherent sources: studying neural interactions in the human brain. Proc. Natl. Acad. Sci. USA *98*, 694–699.
36. Jacobs, J., Miller, J., Lee, S.A., Coffey, T., Watrous, A.J., Sperling, M.R., Sharan, A., Worrell, G., Berry, B., Lega, B., et al. (2016). Direct electrical stimulation of the human entorhinal region and hippocampus impairs memory. Neuron *92*, 983–990.
37. Maris, E., and Oostenveld, R. (2007). Nonparametric statistical testing of EEG- and MEG-data. J.Neurosci. Methods *164*, 177–190.

# STAR★METHODS

## KEY RESOURCES TABLE

| REAGENT or RESOURCE | SOURCE | IDENTIFIER |
|---|---|---|
| Software and Algorithms | | |
| MATLAB 2015b | The MathWorks | https://www.mathworks.com |
| Circular Statistics Toolbox | Berens [26] | https://www.mathworks.com/matlabcentral/fileexchange/10676-circular-statistics-toolbox–directional-statistics- |
| FieldTrip | Oostenveld et al. [27] | http://www.fieldtriptoolbox.org/ |
| Statistical Parametric Mapping 12 | Penny et al. [28] | https://www.fil.ion.ucl.ac.uk/spm/software/spm12/ |
| Advanced Normalization Tools | Avants et al. [29] | http://stnava.github.io/ANTs/ |
| Custom MATLAB scripts | This paper | Request from Lead Contact |
| Other | | |
| Eyelink 1000 | SR Research | https://www.sr-research.com/ |
| Custom MATLAB scripts | This paper | Request from Lead Contact |

## CONTACT FOR REAGENT AND RESOURCE SHARING

Further information and requests for resources and reagents should be directed to and will be fulfilled by the Lead Contact, Tobias Staudigl (tobias.staudigl@cshs.org).

## EXPERIMENTAL MODEL AND SUBJECT DETAILS

36 young healthy adults were included in the MEG study. Initially, 48 participants were recruited; however, 12 dropped out due to not completing the study (7 participants did not come back for one of the sessions, see below), excessive movement artifacts (2 participants) and technical problems during the recordings (3 participants). The 36 participants included in this study (24 females; mean age 23.1 years, range 18-30 years; 35 right handed) reported no history of neurological and/or psychiatric disorders and had normal or corrected-to-normal vision. One participant was excluded from the analysis due to insufficient number of trials. Parts of this data have been published in Staudigl et al. [30] with respect to independent research questions and analyses. All participants gave written informed consent before the start of experiment in accordance with the Declaration of Helsinki. The study was approved by the local ethics committee (commission for human related research CMO-2014/288 region Arnhem/Nijmegen NL).

Additionally, one male patient (age range 25-45) with a history of drug resistant epilepsy was included in the study. The patient, who volunteered to participate in the study at Columbia University Medical School, had depth electrodes implanted for diagnostic reasons. All procedures were approved by the Institutional Review Board at Columbia University Medical School. The patient provided informed consent before participating in the study and was free to withdrawn from the study at any point. The study was approved by the Institutional Review Board at Columbia University Medical School, New York City, US.

## METHOD DETAILS

### Design, Procedure and Materials

The design for the healthy participants comprised an MEG and an fMRI (not reported here) session. The session order was counterbalanced across participants. Three stimulus sets, consisting of 100 photographs each, were constructed for each session. Half of the photographs were outdoor scenes, the other half indoor scenes (see Figure 1A, for an example). The photographs were presented on a 39 × 46 cm back-projection screen in the MEG chamber, subtending a visual angle of approximately 27° × 32°. Two stimulus sets were presented during encoding, all three sets during test. Assignment of set to encoding or test was counterbalanced across participants. Nine additional scenes were presented during a short practice session before encoding and test in order to explain the task. Participants were made aware about the memory test before the start of the experiment. During the study phase, photographs were presented for 4 s. The order was randomized with the constraint that no more than four scenes of the same type (indoor / outdoor) were shown consecutively. The participants were instructed to judge the scene type (indoor / outdoor) via a button press during the fixation cross (variable duration of 1 – 2 s) following each scene (mean accuracy = 0.954, std = 0.068). This encoding task was chosen to ensure attention to each scene. Participants were not expected to fixate, i.e., they freely viewed the scenes. The study phase was followed by a distracter phase (solving simple mathematical problems for ~1 min), ~5 min of fixation to different locations on the screen used to evaluate eye tracker accuracy, and ~1 min of eyes open and ~1 min of eyes closed. Subsequently, participants performed a recognition memory test followed. Only data from the study phase are presented here.

## MEG Acquisition and Preprocessing

MEG was recorded in a magnetically shielded room, using a 275 whole-brain axial gradiometer system (VSM MedTech/CTF MEG, Coquitlam, Canada). The data were sampled at a rate of 1200 Hz following a low-pass anti-aliasing filter with a cutoff at 300 Hz. In addition, we recorded vertical and horizontal electro-oculograms from bipolar Ag/AgCl electrodes (< 10kΩ impedance; available for 32 participants) placed below and above the left eye and at the bilateral outer canthi. 3 head coils placed at anatomical landmarks (nasion and both ear canals) were used to track the position of the head relative to the MEG helmet during the recordings. The head position was continuously monitored using a real-time head localizer [31]. Each participant's nasion, left and right ear canal, and head shape were digitized with a Polhemus 3Space Fasttrack. Data preprocessing was done using the Fieldtrip [27] toolbox. Data were divided into single epochs, ranging from 0 to 4 s after scene onset, and corrected for cardiac artifacts using Independent Component Analysis (ICA).

## Eye Tracking Acquisition, Analyses and Trial Definition

Eye tracking data were recorded simultaneously with MEG data. We tracked the horizontal and vertical movements of each participant's left eye with an Eyelink 1000 (SR Research) eye tracker. The eye tracker was calibrated before recording data, by collecting gaze fixation samples from known target points to map raw eye data onto screen coordinates. Participants fixated nine dots sequentially appearing on a 3 by 3 grid. During the subsequent validation run, the difference between current gaze fixations and fixations during the calibration were obtained. If this difference was smaller than 1 degree visual angle, the calibration was accepted. Vertical and horizontal eye movements were transformed into velocities. Velocities exceeding a given threshold (velocity >6 x the standard deviation of the velocity distribution, duration >12 ms, see Engbert and Kliegl [32]) were defined as saccades. Saccade onsets during scene presentation in the study phase defined the events of interest (trials). Only trials that were free of other saccades and blinks in a 200 ms interval after saccade onset were included. On average, 558 (std = 196.9) trials remained for the analysis. The trials were zero-padded to a length of 0.6 s (i.e., adding 200 ms of zeros before and after the 200 ms of data). One participant was excluded from the analysis due to insufficient number of trials for the hexadirectional analysis.

We focused our analysis on high-frequency activity because it has been shown to correlate with local neural activity [12–15] and was reported in the entorhinal cortex of behaving rodents [16]. We did not analyze lower frequencies (e.g., theta) because our data epochs were too short to obtain a reasonable frequency resolution in these bands.

## Source Reconstruction

Based on our *a priori* hypothesis on the origin of the grid signal in the entorhinal cortex, we performed a region-of-interest based source reconstruction. To account for the spatial resolution of MEG, we constructed two anterior medial temporal ROIs, comprising the anterior portions of the hippocampus and parahippocampal gyrus in the left and right hemisphere, respectively (Figure 1B). For each hemisphere, we aimed at computing one leadfield generated by the entire ROI, rather than averaging across multiple point sources constructed within each ROI, applying a recently optimized MTL source reconstruction method [17].

To construct the anterior medial temporal ROIs, we created 5 mm grids covering the voxels inside the anterior half (median split) of anatomical masks including the labels 'Hippocampus_L', 'ParaHippocampal_L' and 'Hippocampus_R', 'ParaHippocampal_R', respectively, based on the Automatic Anatomical Labeling atlas in Montreal Neurological Institute space [33].

For each participant, the MNI grid was warped onto each participant's anatomy bases on individual structural MR images (1 mm isotropic voxels), acquired on a 3T Siemens Magnetom Prisma MRI system (Siemens, Erlangen, Germany), after aligning the structural images to the MEG coordinate system, utilizing the fiducials (nasion, left and right preauricular points) and individual head-shapes recorded after the experiment. A realistic single-shell brain volume conduction model [34] was constructed for each participant, based on these structural MRIs.

On the basis of this model, the contribution of dipolar sources at each grid point to the sensor level data was estimated. Singular value decomposition was then used to reduce the columns of this sensor-by-grid point leadfield matrix. The vector explaining most variance was selected, resulting in a leadfield matrix consisting of one spatial component for each anterior medial temporal lobe ROI.

The cross-spectral density for the construction of the spatial filters was derived from the Fourier transformation of all trials (epoched 0 to 200 ms from saccade onset) at the frequency of interest (90 Hz) with 30 Hz spectral smoothing using a multitaper approach with 11 tapers from discrete prolate spheroidal sequences (dpss). The cross-spectrum was regularized prior to matrix inversion by loading the diagonal of the matrix with 5% of the average sensor power. We employed the Dynamic Imaging of Coherent Sources (DICS) beamformer [35] to construct a spatial filter for each specified location. The sensor level single-trial data was projected into source space by multiplying it with the spatial filter of each ROI, allowing for further analysis to be conducted in virtual sensor space.

For the whole brain analysis (see Figure 2E), the same source estimation procedure was repeated for all unique labels of the Automatic Anatomical Labeling atlas that include cortical brain areas.

## Hexadirectional analysis

The estimation of the hexadirectional signal followed a two-step procedure (see Figure 1C): First, the putative grid orientation was estimated on one half of the trials (a trial was defined by the onset of individual saccades, see above). Second, aligned and misaligned

(to the estimated putative grid orientation) broadband high-frequency activity (BHA) (60-120 Hz) power was computed. The procedure was repeated with inversed assignment of datasets to the two steps, and aligned and misaligned BHA power was averaged across the repetitions (two-fold cross-validation design).

Because of a horizontal bias in the distribution of saccade directions, we removed trials such that the distribution of saccade directions in the analyses did not differ from a uniform distribution within participants (Rayleigh-test, all p values > 0.05). Performing a 4-,5-,6-,7- and 8-fold analyses of the saccades directions yielded no significant difference between the number of saccades aligned and misaligned to the putative grid orientation (4-fold: $t_{34} = -1.673$, p = 0.104; 5-fold: $t_{34} = -1.202$, p = 0.238; 6-fold: $t_{34} = -0.392$, p = 0.698; 7-fold: $t_{34} = -0.82$, p = 0.418; 8-fold: $t_{34} = -0.986$, p = 0.3310; see Figure S2).

The remaining data was split into halves (set 1, set 2), and BHA power was computed for each set in virtual sensor space by applying a sliding time window approach with a window length of 44 ms length in steps of 10 ms across the data to each trial (epoched from saccade on- to offset, individual for each trial). After multiplying a hanning taper to each window, the Fourier transformation was calculated at the frequency of interest (90 Hz) with 30 Hz spectral smoothing using a multitaper approach with 2 dpss tapers. BHA power was averaged across time bins within each trial, in cases where more than one BHA value resulted from the sliding time window approach.

To estimate the putative grid orientation, regressors (β1, β2) for sine and cosine of saccade directions (Θ) in the respective rotational symmetric space (6-fold symmetry = 60° periodicity) were fitted to set 1 BHA power using a general linear model including the saccade length (sl) as a nuisance regressor:

$$y = \beta_0 + \beta_1 * \cos(6 * \theta) + \beta_2 * \sin(6 * \theta) + \beta_3 * sl + \varepsilon$$

Resulting beta estimates were used to derive the putative grid orientation (Φ):

$$\Phi = \arctan(\beta_2/\beta_1)/symmetry$$

The other half of the data (set 2) was binned according to each trial's saccade direction Θ, into aligned bins (Φ ± 15°, modulo 60°) and misaligned bins (Φ +30° ± 15°, modulo 60°). BHA power was averaged for aligned and misaligned bins, respectively.

After repeating the procedure with inversed assignment of datasets to the two steps, power was averaged across the repetitions for aligned and misaligned bins, respectively. The difference in BHA power (aligned – misaligned) reflects the grid-like modulation of BHA power. Biologically implausible 4-, 5, 7- and 8-fold periodicities were computed with the same approach and compared to the 6-fold periodic modulation of BHA power.

### Intracranial data

One male patient (age range 25-45) with a history of drug resistant epilepsy was included in the study. The patient was implanted with intracranial EEG electrodes for diagnostic purposes. Recordings were performed at the Department of Neurological Surgery, Columbia University, USA. All procedures were approved by the Institutional Review Board at Columbia University Medical School. The patient provided informed consent before participating in the study and was free to withdrawn from the study at any point.

The procedure and design of the study was similar to the MEG procedure and design. The patient performed a free viewing task with 80 colored images (indoor and outdoor sense, faces, animals, etc.) as stimuli. Each image was presented for 6 s in the center of a screen at a distance of about 65 cm, subtending a visual angle of approx. 18° x 12°. The patient was requested to freely view each image. After the stimulus offset a gray screen was displayed with five possible response options. The participant was asked to indicate how he liked the last image on a scale ranging from 1 (very little) to 5 (very much) via button press. The next image was displayed with a jitter interval of 0.1 to 0.5 s.

The locations of the electrodes were determined using pre- and post-operative MRIs and CTs, respectively (for details see Jacobs et al. [36]). One contact was identified to be fully located within the left entorhinal cortex (indicated by red crosshair in Figure S1A) and field potentials from this contact were used for further analysis. To investigate spatial specificity of the hexadirectional modulation, a contact in the amygdala, neighboring the entorhinal cortex (see Figure S1E), was used to as a control site.

Intracranial EEG was recorded from depth electrodes (PMT Corporation) with multiple recording sites (inter-contact spacing = 5 mm), using a Blackrock system (Blackrock Microsystems, Salt Lake City, USA), with voltages referenced to an intracranial electrode site with least signal (2000 Hz sampling rate). Data was re-referenced offline using a bipolar montage. Entorhinal data was re-referenced to the contact's medial neighbor. Amygdala data was re-referenced to its lateral neighbor. A bipolar montage provides high spatial specificity with respect to the underlying electric source and low susceptibility to volume conducted artifacts (e.g., oculomotor artifacts).

Eye movements were monitored with a Tobii TX300 eye tracker. The left and right eye positions were sampled at 300 Hz. A five-point calibration was performed prior to experimental session. Intracranial EEG data was offline downsampled to 1000 Hz and eye tracking data was interpolated to match sampling rate at 1 kHz. Subsequently, eye tracking and intracranial EEG data were co-registered and segmented into epochs with 0.1 s of prestimulus interval and 6 s of stimulus presentation. All epochs were visually inspected for artifacts (e.g., epileptiform spikes). Contaminated epochs were excluded from the analyses. The eye tracking data was low-pass filtered at 30 Hz using a zero-phase forward and reverse butterworth infinite impulse response filter.

Vertical and horizontal eye movements of the left eye were transformed into velocities. Velocities exceeding a given threshold (velocity >6 x the standard deviation of the velocity distribution, duration >12 ms, see Engbert and Kliegl [32]) were defined as

saccades. Saccade onsets during scene presentation in the study phase defined the events of interest (trials). Only trials that were free of other saccades and blinks in a 200 ms interval after saccade onset were included.

Intracranial EEG data were aligned to saccade onsets and BHA power was extracted during saccadic eye movements. The trials were zero-padded to a length of 0.6 s (i.e., adding 200 ms of zeros before and after the 200 ms of data). The estimation of the hexadirectional signal was identical to the procedure described above (see Hexadirectional Analysis).

## QUANTIFICATION AND STATISTICAL ANALYSIS

We tested the null-hypothesis that there is no difference between BHA power for aligned versus misaligned saccade directions, in the left and right ROIs for the 6-fold rotational symmetry, using 2-sided t tests. To control for multiple comparisons, we adopted a significance level of 0.025. To measure effect size Cohen's d was computed as

$$d = \frac{\bar{x}_1 - \bar{x}_2}{\sqrt{s_1^2 + s_2^2 - 2rs_1s_2} \Big/ \sqrt{2(1-r)}}$$

with r denoting Pearson's correlation coefficient.

A 2x5 repeated-measures ANOVA with factors alignment (aligned versus misaligned) and rotational symmetry (4-, 5-, 6-, 7-, and 8-fold) was used to investigate the effect in the left anterior MTL. Planned post hoc comparisons (2-sided t tests, uncorrected) were used to test the difference for the 6-fold symmetry versus the other symmetries (4-, 5-, 7-, and 8-fold) and to test whether BHA power in the left anterior MTL were different from zero for the biologically implausible 4-, 5-, 7-, and 8-fold rotational symmetries.

A further repeated-measures 1-way ANOVA with the factor rotational symmetry (4-, 5-, 6-, 7-, and 8-fold) was used to test for differences among aligned bins in the MEG BHA. To investigate whether the hexadirectional modulation was limited to BHA, a post hoc t test (2-sided, alpha level = 0.05) was performed to test the 60° periodic modulation of power in a lower frequency band (20-50 Hz). As a further post hoc control analysis, two t test (2-sided, alpha = 0.05, uncorrected) were used to test a 60° periodic BHA power modulation recorded on EOG electrodes (for horizontal and vertical EOG signals, respectively). Five post hoc t tests (2-sided, alpha = 0.05, uncorrected) were used to test the difference in number of saccades aligned to the putative grid orientation versus number of saccades misaligned to the putative grid orientation (for 4-, 5-, 6-, 7- and 8-fold rotational symmetries, respectively). All of the above analyses were performed on the group level with N = 35.

We did not include a whole brain statistical approach (as for example implemented in the MEG/EEG Fieldtrip Toolbox), because a significant outcome in this kind of test would only speak to the null hypothesis (no difference between conditions) being rejected and not provide information on the exact spatial extent of the effect [37].

The intracranial BHA power differences (aligned – misaligned) in one patient were statistically quantified by comparing them to a distribution of surrogate BHA power differences. The surrogate distribution of BHA power differences was constructed by randomly assigning trials to the aligned and misaligned condition, respectively. 50000 surrogate BHA power differences were computed. Intracranial BHA power differences were compared to the 50000 surrogate BHA power differences, and considered to be significant if they were larger than the 95% of the surrogate BHA power differences (one-sided test). This procedure was used to quantify the 6-fold periodic modulation of BHA power, as well as the biologically implausible 4-, 5-, 7- and 8-fold periodicities. Additionally, the difference between the hexadirectional modulation of BHA in entorhinal cortex (aligned – misaligned) and amygdala (aligned – misaligned) was compared to a distribution of 50000 surrogate BHA power differences. Differences were considered to be significant if they were larger than the 95% of the surrogate BHA power differences (one-sided test).

## DATA AND SOFTWARE AVAILABILITY

Data and custom-built MATLAB scripts are available from the authors upon request.